2014 IEEE/RSJ International Conference on
Intelligent Robots and Systems (IROS 2014)
September 14-18, 2014, Chicago, IL, USA

Optimized Visibility Motion Planning for Target Tracking and Localization

Hongchuan Wei*, Wenjie Lu*, Pingping Zhu*, Guoquan Huang†, John Leonard‡, and Silvia Ferrari*

Abstract— **This paper presents a visibility-based method for planning the motion of a mobile robotic sensor with bounded field-of-view to optimally track a moving target while localizing itself. The target and robot states are estimated from online sensor measurements and a set of *a priori* known landmarks, using an extended Kalman filter (EKF), and thus the proposed method is applicable to robots without a global positioning system. It is shown that the problem of optimizing the target tracking and robot localization performance is equivalent to optimizing the visibility or probability of detection in the EKF framework under mild assumptions. The control law that maximizes the probability of detection for a robotic sensor with a sector-shaped field-of-view (FoV) is derived as a function of the robot heading and aperture. Simulations have been conducted on synthetic experiments and the results show that the optimized-visibility approach is effective at avoiding target loss, and outperforms a state-of-the-art potential method based on robot trailer models [1].**

I. Introduction

The problem of tracking moving targets using mobile robotic sensors arises in a number of monitoring and surveillance applications [2]–[6]. In many cases, the ability to track and localize the target is limited by the absence of a global positioning system (GPS), and by a bounded field-of-view (FoV) or visibility region, which may cause the sensor to lose the target completely. These difficulties are exacerbated by the need for tracking moving targets in complex unstructured environments, in which target loss may cause unbounded tracking errors if the lost target can not be retrieved. Furthermore, since the position and orientation of the sensor FoV is determined by the control inputs, the motion of the robotic sensor must be planned in concert with its measurement sequence for both sensing and navigation objectives to be optimized [7], [8].

An optimized robot motion planning algorithm has been recently proposed in [9] for leader-follower formation problems in which the follower seeks to minimize the uncertainty in its relative position and heading with respect to the leader. A gradient-based active target-tracking method for robots equipped with 3D range finder sensors was proposed in [10] for minimizing the uncertainty in robot and target position estimates. These methods, however, do not account for bounded FoVs, but assume the target is always within range of the sensor. Cell decomposition [11], [12], probabilistic roadmap methods [13], [14], and potential field methods [15] have been proposed for planning the motion of a robotic sensor with a bounded FoV in order to optimize its ability to classify *stationary* targets, in an obstacle-populated environment. Geometric transversal methods have been developed for planning the motion of omnidirectional sensors such that their probability of detecting a moving target is optimized [8], [16], [17]. Other visibility-based methods that account for both the sensor kinodynamic constraints and bounded FoV have been proposed in [18]–[22]. However, all of these methods assume that the sensor state with respect to an inertial frame of reference is perfectly known at all times.

To address the aforementioned issues, an optimized-visibility motion planning approach is proposed using an extended Kalman filter (EKF) to simultaneously track the target and localize the robotic sensor [23]–[25]. Within this estimation framework, a control law is derived analytically by assuming the FoV of the exteroceptive sensor can be approximated by a sector with a fixed orientation with respect to the robot and a fixed aperture. Note that the proposed optimized-visibility approach is applicable to any robot that is equipped with exteroceptive sensors, such as laser scanner or camera, for tracking and localizing moving targets, and proprioceptive sensors, such as odometer, for providing ego-motion information. The results show that the proposed method is effective at tracking and localizing a moving target with low target loss rates, and outperforms a state-of-the-art potential method based on robot trailer models [1].

II. Problem Formulation

Consider a mobile robotic sensor, hereon referred to as robot, deployed to track a moving target in a 2D workspace, $\mathcal{W} \subset \mathbb{R}^2$, that is convex [26]. The robot kinematics in $\mathcal{W}$ can be described by the unicycle motion model [27],

$$\dot{\mathbf{q}}_r = \begin{bmatrix} \cos\theta_r & 0 \\ \sin\theta_r & 0 \\ 0 & 1 \end{bmatrix} \mathbf{u}_r \tag{1}$$

where $\mathbf{q}_r = [x_r \quad y_r \quad \theta_r]^T$ is the robot configuration or *state* with respect to an inertial (or global) frame of reference $\mathcal{F}_\mathcal{W}$, $\mathbf{u}_r = [v_r \quad \omega_r]^T$ is the robot control vector, v_r denotes the translational speed, ω_r is the angular velocity, and $\mathbf{u}_r \in \mathcal{U}$, where $\mathcal{U} = [v_{\min},\ v_{\max}] \times [\omega_{\min},\ \omega_{\max}]$ is the space of admissible control inputs.

Assume the robot velocity and heading remain constant during every time interval δt, and let k denote the discrete time index. Then, the robot state propagation equations can

*Laboratory for Intelligent Systems and Controls (LISC), Duke University, Durham, NC 27708.
†Department of Mechanical Engineering, University of Delaware, Newark, DE 19716.
‡Computer Science and Artificial Intelligence Laboratory (CSAIL), Massachusetts Institute of Technology (MIT), Cambridge, MA 02139.
E-mail:{hongchuan.wei, wenjie.lu, pingping.zhu, sferrari}@duke.edu, ghuang@csail.mit.edu, jleonard@mit.edu.

be obtained as follows [28],

$$\mathbf{q}_r(k+1) \triangleq \mathbf{f}_r[\mathbf{q}_r(k), \mathbf{u}_r(k), k] = \mathbf{q}_r(k) + \mathbf{B}_r(k)\mathbf{u}_r(k), \quad (2)$$

where

$$\mathbf{B}_r(k) = \begin{bmatrix} \cos\theta_r(k)\delta t & 0 \\ \sin\theta_r(k)\delta t & 0 \\ 0 & \delta t \end{bmatrix}. \quad (3)$$

The proprioceptive sensor (e.g. odometer) obtains noisy measurements of the control vector,

$$\mathbf{z}_r(k) \triangleq \mathbf{h}_r[\mathbf{u}_r(k)] = \mathbf{u}_r(k) + \mathbf{v}_r(k), \quad (4)$$

where $\mathbf{v}_r(k)$ is white Gaussian noise with a time-invariant and known covariance matrix $\mathbf{Q}_r$, i.e., $\mathbf{v}_r(k) \sim \mathcal{N}(\mathbf{0}, \mathbf{Q}_r)$.

The robot is also equipped with an exteroceptive sensor characterized by a sector-shaped FoV, denoted by $\mathcal{S} \subset \mathcal{W}$, that is rigidly connected to the robot, and has an aperture or central angle α, and a range or radius γ, as shown in Fig.1. Then, the motion of any point in $\mathcal{S}$ can be described by the robot configuration vector $\mathbf{q}_r$, which includes the robot inertial position $\mathbf{x}_r = [x_r \quad y_r]^T$, and heading θ_r. Let the target state be denoted by $\mathbf{q}_t = [x_t \quad y_t \quad \dot{x}_t \quad \dot{y}_t]^T$, where $\mathbf{x}_t = [x_t \quad y_t]^T$ is the target position, and $\dot{\mathbf{x}}_t = [\dot{x}_t \quad \dot{y}_t]^T$ is the target velocity. When the target is inside the FoV, the exteroceptive sensor can measure its relative distance and bearing according to the model,

$$\mathbf{z}_t \triangleq \mathbf{h}_t(\mathbf{q}_r, \mathbf{q}_t) = \begin{cases} [\rho_t \quad \theta_t]^T + \mathbf{v}_t, & \mathbf{x}_t \in \mathcal{S}(\mathbf{q}_r) \\ \emptyset, & \mathbf{x}_t \notin \mathcal{S}(\mathbf{q}_r) \end{cases} \quad (5)$$

where $\rho_t = \|\mathbf{x}_r - \mathbf{x}_t\|$ denotes the Euclidean distance between $\mathbf{x}_r$ and $\mathbf{x}_t$, θ_t is the angle between the robot heading and the direction from robot to target. $\mathbf{v}_t$ is zero-mean Gaussian noise with covariance $\mathbf{R}_t$. The workspace $\mathcal{W}$ is populated with L stationary landmarks with positions $\mathbf{x}_l = [x_1 \quad y_1 \quad \ldots \quad x_L \quad y_L]^T$ that can be used to aid localization. The measurement of the landmarks also consists of the relative distance and bearing,

$$\mathbf{z}_{l_i} \triangleq \mathbf{h}_l(\mathbf{q}_r, \mathbf{x}_{l_i}) = \begin{cases} [\rho_{l_i} \quad \theta_{l_i}]^T + \mathbf{v}_l, & \mathbf{x}_{l_i} \in \mathcal{S}(\mathbf{q}_r) \\ \emptyset, & \mathbf{x}_{l_i} \notin \mathcal{S}(\mathbf{q}_r) \end{cases} \quad (6)$$

for $i = 1, \ldots, L$, where $\rho_{l_i} = \|\mathbf{x}_r - \mathbf{x}_{l_i}\|$ and θ_{l_i} is the relative angle between the robot heading and the ith landmark location. $\mathbf{v}_l$ is zero-mean Gaussian noise with covariance $\mathbf{R}_l$.

The target motion in $\mathcal{W}$ is assumed governed by a linear stochastic motion model that, in discrete time, can be written as a difference equation,

$$\mathbf{q}_t(k+1) \triangleq \mathbf{f}_t[\mathbf{q}_t(k)] + \mathbf{G}\mathbf{w} = \mathbf{\Phi}_t\mathbf{q}_t(k) + \mathbf{G}\mathbf{w}, \quad (7)$$

where $\mathbf{w}$ is zero-mean white Gaussian noise with covariance matrix $\mathbf{Q}_t$, $\mathbf{\Phi}_t$ is the state transition matrix, and $\mathbf{G}$ is the noise Jacobian matrix, both of which are assumed to be time invariant and known *a priori*.

Based on the above robot and target motion model, and the latest proprioceptive and exteroceptive measurements, $\mathbf{z}_r(k)$, $\mathbf{z}_t(k)$ and $\mathbf{z}_l(k)$, the goal is to obtain a control law for the unicycle robot (1) such that its ability to track and localize the target (7) is optimized without losing the target. The sensor tracking and localization accuracy, presented in Section IV-A, are obtained from the EKF presented in the next section.

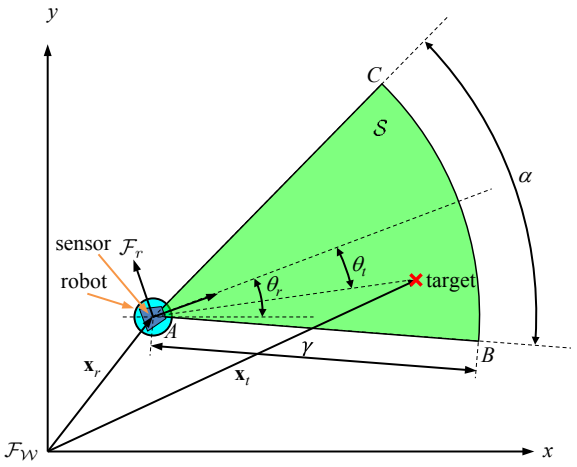

Fig. 1. FoV of exteroceptive sensor.

III. EKF-based Robot Localization and Target Tracking

In the absence of GPS or other information on the robot position in inertial frame, an EKF can be used to estimate both the robot and the target state from the proprioceptive and exteroceptive measurements described in the previous section. Consider an augmented state vector containing both the robot and the target state,

$$\mathbf{q}(k) = [\mathbf{q}_r^T(k) \quad \mathbf{q}_t^T(k)]^T, \quad (8)$$

and the augmented control vector

$$\mathbf{u}(k) = [\mathbf{u}_r^T(k) \quad \mathbf{0}]^T. \quad (9)$$

Based on the robot state propagation equation (2) and the target state propagation equation (7), the joint state propagation of the robot and the target is

$$\mathbf{q}(k+1) = \mathbf{f}[\mathbf{q}(k), \mathbf{u}(k), k] = \begin{bmatrix} \mathbf{f}_r[\mathbf{q}_r(k), \mathbf{u}_r(k), k] \\ \mathbf{f}_t[\mathbf{q}_t(k)] \end{bmatrix} \quad (10)$$

and the Jacobian matrix of the state transition function for the joint state is

$$\mathbf{\Phi} = \begin{bmatrix} \mathbf{\Phi}_r(k) & \mathbf{0} \\ \mathbf{0} & \mathbf{\Phi}_t \end{bmatrix}, \quad (11)$$

where

$$\mathbf{\Phi}_r(k) \triangleq \frac{\partial}{\partial \mathbf{q}_r(k)}\{\mathbf{f}_r[\mathbf{q}_r(k), \mathbf{u}_r(k), k]\} = \begin{bmatrix} 1 & 0 & -\sin\theta_r(k)v_r(k)\delta t \\ 0 & 1 & \cos\theta_r(k)v_r(k)\delta t \\ 0 & 0 & 1 \end{bmatrix}. \quad (12)$$

In the EKF, the prediction of the joint state and its

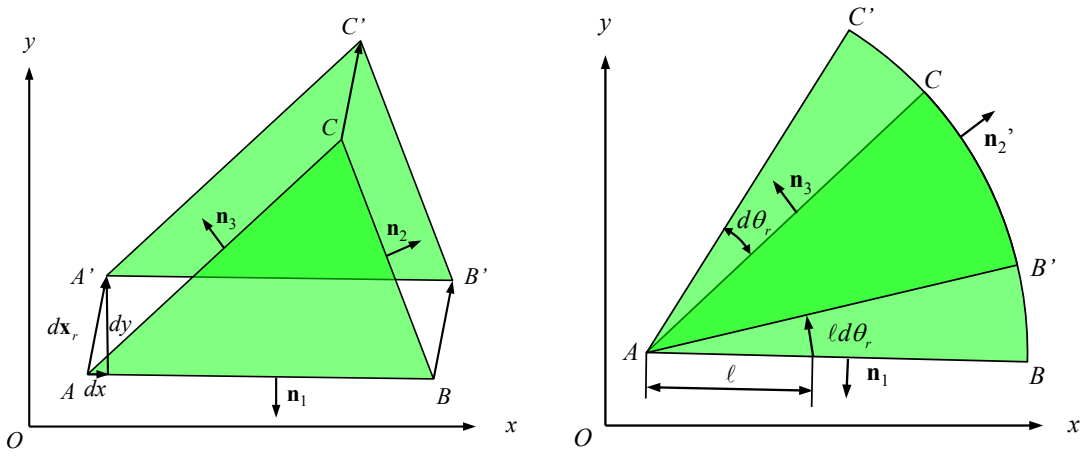

(a) translation (b) rotation

Fig. 2. Illustration of the changes of the robot FoV due to the translation and rotation of the robot.

covariance before the measurements is given by,

$$\hat{\mathbf{q}}(k+1|k) = \mathbf{f}[\hat{\mathbf{q}}(k|k), \mathbf{u}(k), k] \tag{13}$$

$$\mathbf{P}(k+1|k) = \mathbf{\Phi}\mathbf{P}(k|k)\mathbf{\Phi}^T + \begin{bmatrix} \mathbf{B}_r(k)\mathbf{Q}_r\mathbf{B}_r^T(k) & \mathbf{0} \\ \mathbf{0} & \mathbf{G}\mathbf{Q}_t\mathbf{G}^T \end{bmatrix} \tag{14}$$

The Jacobian matrix of the measurement function $\mathbf{h} \triangleq [\mathbf{h}_t^T \quad \mathbf{h}_l^T]^T$ is [23]

$$\mathbf{H}(k) = \begin{bmatrix} \frac{2(x_r-x_t)}{\|\mathbf{x}_r-\mathbf{x}_t\|} & \frac{2(y_r-y_t)}{\|\mathbf{x}_r-\mathbf{x}_t\|} & 0 & \frac{2(x_t-x_r)}{\|\mathbf{x}_r-\mathbf{x}_t\|} & \frac{2(y_t-y_r)}{\|\mathbf{x}_r-\mathbf{x}_t\|} & 0 \\ 0 & 0 & 1 & 0 & 0 & 1 \\ \frac{2(x_r-x_1)}{\|\mathbf{x}_r-\mathbf{x}_{l_1}\|} & \frac{2(y_r-y_1)}{\|\mathbf{x}_r-\mathbf{x}_{l_1}\|} & 0 & 0 & 0 & 0 \\ 0 & 0 & 1 & 0 & 0 & 0 \\ & & \vdots & & & \\ \frac{2(x_r-x_L)}{\|\mathbf{x}_r-\mathbf{x}_{l_L}\|} & \frac{2(y_r-y_L)}{\|\mathbf{x}_r-\mathbf{x}_{l_L}\|} & 0 & 0 & 0 & 0 \\ 0 & 0 & 1 & 0 & 0 & 0 \end{bmatrix} \tag{15}$$

The EKF posterior estimates are computed as follows [29]:

$$\tilde{\mathbf{y}}(k+1) = \begin{bmatrix} \mathbf{z}_r^T(k+1) \\ \mathbf{z}_l^T(k+1) \end{bmatrix} - \mathbf{h}[\hat{\mathbf{q}}(k+1|k)] \tag{16}$$

$$\mathbf{S}(k+1) = \mathbf{H}(k+1)\mathbf{P}(k+1|k)\mathbf{H}(k+1)^T + \begin{bmatrix} \mathbf{R}_r & \mathbf{0} \\ \mathbf{0} & \text{diag}([\mathbf{R}_t \quad \dots \quad \mathbf{R}_t]) \end{bmatrix} \tag{17}$$

$$\mathbf{K}(k+1) = \mathbf{P}(k+1|k)\mathbf{H}(k+1)^T\mathbf{S}^{-1}(k+1) \tag{18}$$

$$\hat{\mathbf{q}}(k+1|k+1) = \hat{\mathbf{q}}(k+1|k) + \mathbf{K}(k+1)\tilde{\mathbf{y}}(k+1) \tag{19}$$

$$\mathbf{P}(k+1|k+1) = [\mathbf{I} - \mathbf{K}(k+1)\mathbf{H}(k+1)]\mathbf{P}(k+1|k) \tag{20}$$

where diag$(\cdot)$ denotes the square diagonal matrix with the blocks of matrices on the main diagonal.

IV. Visibility-based Robot Motion Planning

This section presents a motion planning method for optimizing the tracking and localization performance of the exteroceptive robotic sensor described in Section II, based on the output of the EKF algorithm presented in Section III. In what follows, an objective function, representing the sensor performance, is first presented. Then, a control law that optimizes the sensor performance by guiding the robot to obtain the best next measurements is derived.

A. Tracking and Localization Performance

In GPS-denied environments, the quality of target state estimates depends on the estimates of the robot state, obtained by the EKF algorithm. Therefore, the overall target tracking and localization performance can be represented by the expected power of the error between the true and estimated robot-target joint states. For sensors with limited FoV, it is possible to obtain an empty target measurement. Therefore, two situations are considered for calculating the joint state error: when the target measurement is available, the posterior estimate of the joint state, $\hat{\mathbf{q}}(k+1|k+1)$, is used; otherwise, the prior estimate, $\hat{\mathbf{q}}(k+1|k)$, is employed. Let P_d denote the probability that the target measurement is available, the error power can be obtained as follows,

$$\begin{aligned} J[\mathbf{u}_r(k)] = {} & \mathbb{E}\left[\mathbf{e}(k+1|k)^T\mathbf{e}(k+1|k)\right] \times (1-P_d) \\ & + \mathbb{E}\left[\mathbf{e}(k+1|k+1)^T\mathbf{e}(k+1|k+1)\right] \times P_d \end{aligned} \tag{21}$$

where,

$$\mathbf{e}(k+1|k) = \mathbf{q}(k) - \hat{\mathbf{q}}(k+1|k), \tag{22}$$

$$\mathbf{e}(k+1|k+1) = \mathbf{q}(k) - \hat{\mathbf{q}}(k+1|k+1), \tag{23}$$

and $\mathbb{E}(\cdot)$ denotes the expectation.

To derive P_d, we integrate the target state distribution over the robotic sensor's FoV,

$$P_d[\mathbf{q}_r(k)] = \int_{\mathcal{S}[\mathbf{q}_r(k)]} f_t[\mathbf{x}_t(k)]d\mathbf{x}_t(k) \tag{24}$$

$f_t[\mathbf{x}_t(k)]$ is the probability density function (PDF) of target state distribution, which can be approximated by a Gaussian distribution, as follows,

$$\begin{aligned} f_t[\mathbf{x}_t(k)] &= \mathcal{N}[\mathbf{x}_t(k); \hat{\mathbf{x}}_t(k|k-1), \mathbf{P}_t(k|k-1)] \\ &\triangleq \mathcal{N}[\mathbf{x}_t(k); \boldsymbol{\mu}_t(k), \mathbf{\Sigma}_t(k)], \end{aligned} \tag{25}$$

where, $\boldsymbol{\mu}_t(k)$ and $\boldsymbol{\Sigma}_t(k)$ are introduced to simplify our ensuing derivations. Then (21) can be rewritten as

$$J[\mathbf{u}_r(k)] = \text{tr}[\mathbf{P}(k+1|k)] - P_d \times \{\text{tr}[\mathbf{P}(k+1|k)] - \text{tr}[\mathbf{P}(k+1|k+1)]\} \tag{26}$$

where $\text{tr}(\cdot)$ denotes the trace of a matrix. Since the propagation step of EKF produces prior estimate of the joint state only, in this paper we focus on controlling robot to get the most informative measurements to reduce the uncertainty of the joint state. Therefore, it is assumed that the prior estimates are optimal with respect to the robot control. In addition, for the priori and posteriori state estimates in the EKF, it is true that

$$\text{tr}[\mathbf{P}(k+1|k)] - \text{tr}[\mathbf{P}(k+1|k+1)] \geq 0. \tag{27}$$

As a result, minimizing the error of the joint state (21) can be achieved by maximizing the probability of detection (24), and the robot control law can be obtained by solving the following constrained optimization problem in $\mathbf{u}_r(k)$:

$$\max_{\mathbf{u}_r(k)} \quad P_d[\mathbf{q}_r(k+1)] \tag{28}$$

$$\text{s.t.} \quad \mathbf{q}_r(k+1) = \mathbf{q}_r(k) + \mathbf{B}_r(k)\mathbf{u}_r(k)\delta t \tag{29}$$

B. Robot Control Law

A robot control law that takes into account the tracking and localization performance presented in Section IV-A and the models in Section II, while being characterized by low computational complexity so as to afford realtime implementation can be obtained as follows.

At any discrete time step k, the robot control inputs are computed so as to maximize the probability of detection at the next time step, $(k+1)$, subject to the robot kinematics. The solution of the constrained optimization problem (28-29) can be obtained by moving in the direction of the adjoined gradient which, in this case, can be obtained analytically, thus providing the control law in closed form. As a first step, the Jacobian for (28) can be written as,

$$\frac{\partial P_d[\mathbf{q}_r(k+1)]}{\partial \mathbf{u}_r(k)} = \frac{\partial P_d[\mathbf{q}_r(k+1)]}{\partial \mathbf{q}_r(k+1)} \frac{\partial \mathbf{q}_r(k+1)}{\partial \mathbf{u}_r(k)}. \tag{30}$$

where

$$\frac{\partial P_d[\mathbf{q}_r(k+1)]}{\partial \mathbf{q}_r(k+1)} = \begin{bmatrix} \frac{\partial}{\partial x_r}\{P_d[\mathbf{q}_r(k+1)]\} \\ \frac{\partial}{\partial y_r}\{P_d[\mathbf{q}_r(k+1)]\} \\ \frac{\partial}{\partial \theta_r}\{P_d[\mathbf{q}_r(k+1)]\} \end{bmatrix}. \tag{31}$$

Each term of the above expression (31) is computed by derivatives of integrals. For example, if the robot's FoV is approximated by a triangle ABC as in Fig. 2, the first entry of (31) can be calculated as follows:

$$\begin{aligned} \frac{\partial}{\partial x_r} P_d[\mathbf{q}_r(k+1)] &= \frac{\partial}{\partial x_r} \int_{\mathcal{S}[\mathbf{q}_r(k+1)]} f_t(\mathbf{x}_t) d\mathbf{x}_t \\ &= \int_{\mathcal{S}[\mathbf{q}_r(k+1)]} \frac{\partial}{\partial x_r} f_t(\mathbf{x}_t) d\mathbf{x}_t + \oint_{\partial\mathcal{S}[\mathbf{q}_r(k+1)]} (\mathbf{v}_x \cdot \mathbf{n}) f_t(\mathbf{x}_t) d\mathbf{x}_t \end{aligned} \tag{32}$$

where $\partial\mathcal{S}$ denotes the boundary of $\mathcal{S}$, and $\cdot$ denotes the inner product. $\mathbf{v}_x = [1 \quad 0]^T$ is the velocity of the robot FoV. $\mathbf{n}$ represents the outward-pointing unit normal vector along the boundary of the robot FoV. The outward-pointing unit normal vectors can be obtained through the heading of the robot and the opening angle of the robot FoV, as shown in Fig. 2 (a), i.e.,

$$\begin{aligned} \mathbf{n}_1 &= \mathbf{C}(\pi/2 + \alpha/2)[\cos\theta_r \quad \sin\theta_r]^T \\ \mathbf{n}_2 &= [\cos\theta_r \quad \sin\theta_r]^T \\ \mathbf{n}_3 &= \mathbf{C}(-\pi/2 - \alpha/2)[\cos\theta_r \quad \sin\theta_r]^T \end{aligned} \tag{33}$$

where $\mathbf{C}(\cdot)$ is the 2×2 rotation matrix. Moreover, since $f_t(\mathbf{x}_t)$ is not a function of $\mathbf{q}_r$, $\frac{\partial}{\partial \mathbf{q}_r} f_t(\mathbf{x}_t) = 0$. In addition, (25) gives the analytical form of f_t. Then the partial derivative in (32) can be simplified as follows,

$$\begin{aligned} &\frac{\partial}{\partial x_r} P_d[\mathbf{q}_r(k+1)] \\ &= \int_{AB} (\mathbf{v}_x \cdot \mathbf{n}_1) \exp[-\frac{1}{2}(\mathbf{x}_t - \boldsymbol{\mu}_t)^T \boldsymbol{\Sigma}_t^{-1} (\mathbf{x}_t - \boldsymbol{\mu}_t)] d\mathbf{x}_t \\ &+ \int_{BC} (\mathbf{v}_x \cdot \mathbf{n}_2) \exp[-\frac{1}{2}(\mathbf{x}_t - \boldsymbol{\mu}_t)^T \boldsymbol{\Sigma}_t^{-1} (\mathbf{x}_t - \boldsymbol{\mu}_t)] d\mathbf{x}_t \\ &+ \int_{CA} (\mathbf{v}_x \cdot \mathbf{n}_3) \exp[-\frac{1}{2}(\mathbf{x}_t - \boldsymbol{\mu}_t)^T \boldsymbol{\Sigma}_t^{-1} (\mathbf{x}_t - \boldsymbol{\mu}_t)] d\mathbf{x}_t \end{aligned} \tag{34}$$

Similarly, the second entry of (31) can be obtained in the same way, except that $\mathbf{v}_y = [0 \quad 1]^T$, as follows,

$$\begin{aligned} &\frac{\partial}{\partial y_r} P_d[\mathbf{q}_r(k+1)] \\ &= \int_{AB} (\mathbf{v}_y \cdot \mathbf{n}_1) \exp[-\frac{1}{2}(\mathbf{x}_t - \boldsymbol{\mu}_t)^T \boldsymbol{\Sigma}_t^{-1} (\mathbf{x}_t - \boldsymbol{\mu}_t)] d\mathbf{x}_t \\ &+ \int_{BC} (\mathbf{v}_y \cdot \mathbf{n}_2) \exp[-\frac{1}{2}(\mathbf{x}_t - \boldsymbol{\mu}_t)^T \boldsymbol{\Sigma}_t^{-1} (\mathbf{x}_t - \boldsymbol{\mu}_t)] d\mathbf{x}_t \\ &+ \int_{CA} (\mathbf{v}_y \cdot \mathbf{n}_3) \exp[-\frac{1}{2}(\mathbf{x}_t - \boldsymbol{\mu}_t)^T \boldsymbol{\Sigma}_t^{-1} (\mathbf{x}_t - \boldsymbol{\mu}_t)] d\mathbf{x}_t \end{aligned} \tag{35}$$

Let $\text{sign}(\cdot)$ denote the sign function, and ℓ denote the distance from a point on the boundary of the FoV to the point A. Then, the third entry of (31) can also be calculated analytically as follows,

$$\begin{aligned} &\frac{\partial}{\partial \theta_r} P_d[\mathbf{x}_r(k+1)] \\ &= \int_{AB} -\text{sign}(d\theta_r)\ell \exp[-\frac{1}{2}(\mathbf{x}_t - \boldsymbol{\mu}_t)^T \boldsymbol{\Sigma}_t^{-1} (\mathbf{x}_t - \boldsymbol{\mu}_t)] d\mathbf{x}_t \\ &+ \int_{CA} \text{sign}(d\theta_r)\ell \exp[-\frac{1}{2}(\mathbf{x}_t - \boldsymbol{\mu}_t)^T \boldsymbol{\Sigma}_t^{-1} (\mathbf{x}_t - \boldsymbol{\mu}_t)] d\mathbf{x}_t \end{aligned} \tag{36}$$

Now let us consider the the second term of (30), which essentially is the robot motion model, i.e.,

$$\frac{\partial \mathbf{q}_r(k+1)}{\partial \mathbf{u}_r(k)} = \mathbf{B}_r(k)\delta t \tag{37}$$

Thus, we have computed the Jacobian (34)-(37). The

Procedure FindOptimalControl$\big(f_t(\mathbf{x}_t),\, \mathcal{U},\, \epsilon\big)$

$\mathbf{u}_r = \mathbf{u}_0$
while(1)
  $\mathbf{u}'_r \leftarrow \mathbf{u}_r + \eta \frac{\partial}{\partial \mathbf{u}_r(k)} \{P_d[\mathbf{q}_r(k+1)]\}$
  if $\mathbf{u}'_r \notin \mathcal{U}$
    break
  elseif $\|\mathbf{u}'_r - \mathbf{u}_r\| \leq \epsilon$
    break
  else
    $\mathbf{u}_r \leftarrow \mathbf{u}'_r$
  endif
endwhile
return $\mathbf{u}_r$

Alg.1 Implementation of the optimized-visibility method

optimized-visibility method is summarized in Alg. 1, where η is the learning rate and ϵ is a predefined threshold [30]. Notice that Alg. 1 does handle the situation when the target is out of the FoV for multiple steps since this paper focuses on analyzing the ability of avoiding target loss.

V. Simulation Results

In order to validate the effectiveness of the proposed approach, we conduct various simulations under different conditions, and compare the performance to that of a state-of-the-art potential field approach, which controls the robot as a trailer [1]. Specifically, it first calculates a force, $\mathbf{f}_p(k)$, proportional to the distance between the center of the inscribed circle of the FoV, $\mathbf{x}_p(k)$, and the estimated mean of target position distribution, $\boldsymbol{\mu}_t(k)$.

$$\mathbf{f}_p(k) = c_p \|\mathbf{x}_p(k) - \boldsymbol{\mu}_t(k)\|, \tag{38}$$

where c_p is a constant. Then, the potential approach projects the force along the robot heading and perpendicular to the robot heading. Let $\theta_p(k)$ denote the angle between the robot heading and the direction from $\mathbf{x}_p(k)$ to $\boldsymbol{\mu}_t(k)$. The control is determined as a linear function of the projections, such that

$$v_r(k) = a_p \|\mathbf{f}_p(k)\| \cos\theta_p(k) \tag{39}$$

$$\omega_r(k) = b_p \|\mathbf{f}_p(k)\| \sin\theta_p(k) \tag{40}$$

where a_p and b_p are constants.

For the results presented in Fig. 3 and Fig. 4, the robot and the target are assumed to move in a workspace of $\mathcal{W} = [-50, 50] \times [-50, 50]$ m^2. The sensor's FoV is assumed to have a radius, $\gamma = 2.5$ m, and an opening angle, $\alpha = \pi/6$ rad. This choice of parameters results in a relative small sensor's FoV as compared to the workspace, so that target is easy to disappear from the FoV. The sampling time, δt, is assumed to be 0.2 sec, which means the robot makes both the proprioceptive measurements, $\mathbf{z}_r(k)$, and the exteroceptive measurements, $\mathbf{z}_t(k)$, every 0.2 second. For the proprioceptive measurements, the noise is 2% of the maximum speed the robot can travel at and $\pi/180$ rad/sec for the angular speed measurement. In all the tests, it is assumed that the maximum speed that the robot is able to achieve is 3 m/sec, and the maximum angular speed for the robot is 0.5 rad/sec. As a result, the proprioceptive noise covariance is $\mathbf{R}_r \approx \text{diag}([36 \quad 3]) \times 10^{-4}$. Note that we did not restrict the robot to travel forward, which means the robot can travel backward and reach the speed limit of 3 m/sec. For the exteroceptive measurements, the noise level is 3% of the maximum detection radius of the FoV for the range measurement, and $\pi/36$ rad for the bearing measurement, and the noise covariance is $\mathbf{R}_t \approx \text{diag}([81 \quad 76]) \times 10^{-4}$.

In this test, the target adopts a constant velocity model:

$$\boldsymbol{\Phi}_t = \begin{bmatrix} 1 & 0 & \delta t & 0 \\ 0 & 1 & 0 & \delta t \\ 0 & 0 & 1 & 0 \\ 0 & 0 & 0 & 1 \end{bmatrix}. \tag{41}$$

The noise in the target state propagation equation (7) makes the target move randomly in the workspace. It is assumed that $\mathbf{G} = \mathbf{I}$ and the noise of the target position is correlated with its speed. The noise matrix is assumed to be

$$\mathbf{Q} = \begin{bmatrix} \delta t^3\sigma^2/3 & 0 & \delta t^2\sigma^2/2 & 0 \\ 0 & \delta t^3\sigma^2/3 & 0 & \delta t^2\sigma^2/2 \\ \delta t^2\sigma^2/2 & 0 & \delta t\sigma^2 & 0 \\ 0 & \delta t^2\sigma^2/2 & 0 & \delta t\sigma^2 \end{bmatrix}, \tag{42}$$

where σ is chosen to be 0.5 m/sec, which is large enough to prevent the target from moving in a straight line. The initial state of the target is assumed to be $\mathbf{q}_t(0) = [0 \quad 0 \quad 0 \quad 0]$, which enables the target to move in every direction with the same probability.

Figure 3(a) shows the tracking performance of the proposed gradient descent approach in one particular realization, for $\eta = 1$ and $\epsilon = 10^{-3}$, from which it is clear that the robot is able to track the target throughout the simulation. With the identical setup, the tracking result of the potential method is shown in Fig. 3(b). As evident, the robot lost the target at time step $k = 170$, while the proposed optimized visibility approach reliably tracks the target (see Fig. 3(a)). Figure 4 shows comparison between the estimated and true target trajectories. The deviation of estimated target trajectory from the true target trajectory decreases.

To further justify the result in Fig. 3, we have performed various simulations with different parameters. In particular, we studied the impact of FoV opening angle α and the radius γ on the efficiency of the potential and the proposed optimized visibility methods. In order to evaluate the tracking performance, the percentage of target detection, β, is defined as the number of successful target detections divided by the total number of simulation steps. The parameter η is set to one for all the simulations and ϵ is 10^{-3}. Ten Simulations are conducted for every scenario. The mean and one standard variance are summarized in Fig. 5 and Fig. 6, which show that the optimized visibility approach outperforms the potential method with higher detection percentage.

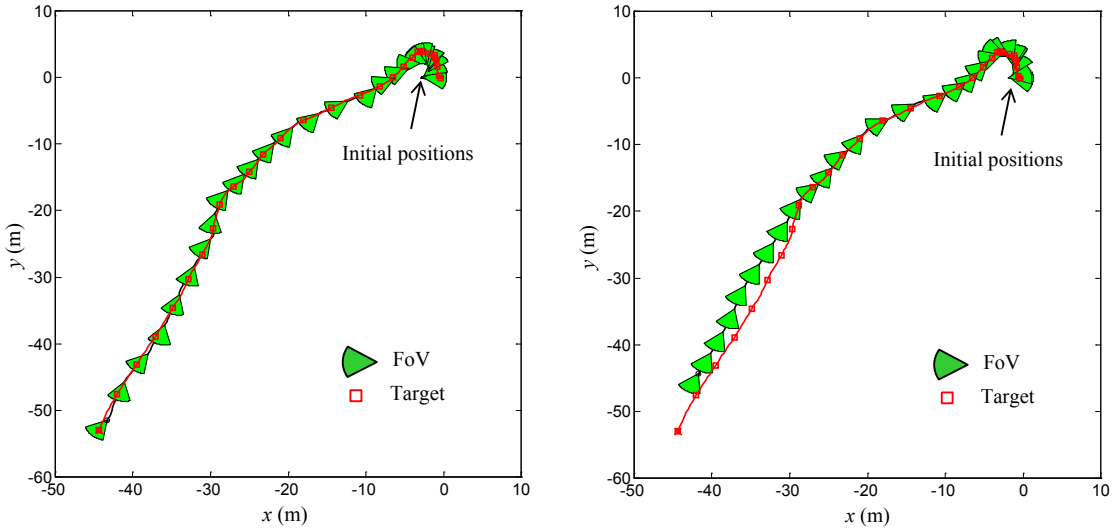

(a) optimized-visibility approach (b) potential approach

Fig. 3. An example of the simulation result where the visibility optimized approach tracks enables the robot to keep the target in its FoV all the time while the potential field method loses the target around 200 time step, for a FoV with $\alpha = \pi/6$ rad and $\gamma = 2.5$ m.

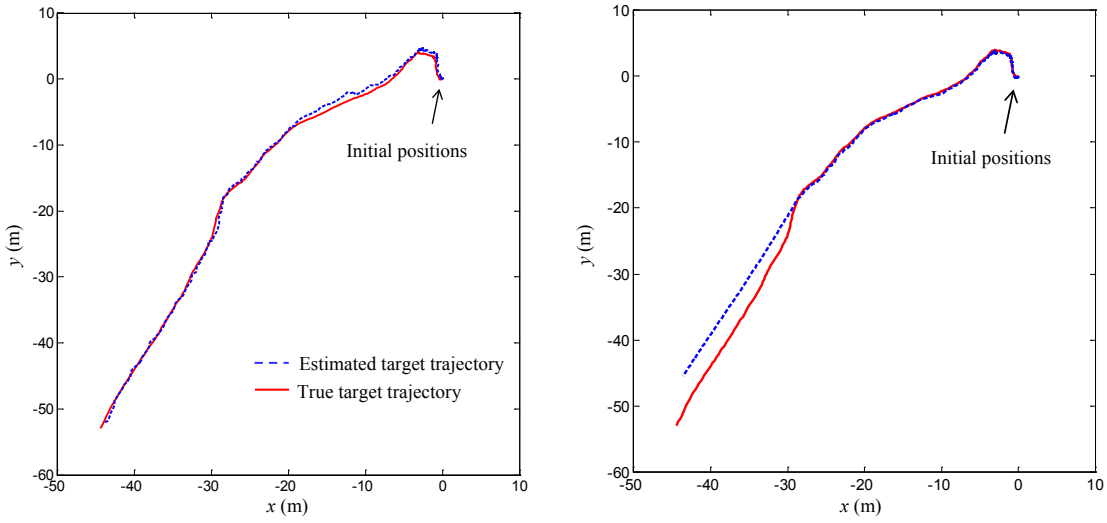

(a) optimized-visibility approach (b) potential approach

Fig. 4. The estimated and true target trajectories obtained by the optimized visibility approach and the potential field approach for the example in Fig. 3.

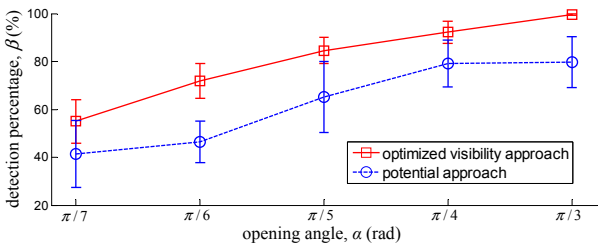

Fig. 5. Percentage of detections obtained by the proposed optimized visibility and the potential approaches for various opening angles.

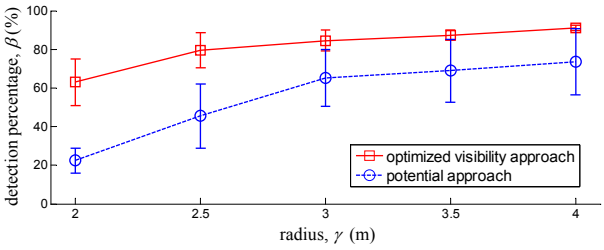

Fig. 6. Percentage of detections obtained by the proposed optimized visibility and the potential approaches for various edge lengths.

VI. Conclusions and Future Work

In this paper, we have studied the problem of target tracking using mobile robots (sensors), by focusing on optimal motion planning for the tracking robots in order to achieve best tracking performance. In particular, within the EKF framework of jointly estimating the robot pose and target

state, the robot motion planning problem has been formulated as maximizing the target-detection probability. Furthermore, an optimized visibility approach for solving this optimization problem has been introduced, which is derived analytically based on the optimality condition. Numerical simulation results have demonstrated that the proposed approach outperforms the state-of-the-art potential approach.

In future work, the current one-step-ahead optimization will be extended to the multiple-step-ahead cases, and the proposed optimized visibility method will be generalized to the problem of simultaneous localization, mapping, and target tracking, which is particularly important for mobile robots working in dynamic environments. Moreover, different estimation algorithms will be investigated for a given application where the EKF may not be sufficient (e.g., it is degraded due to larger linearization errors). In particular, it is noted that the recently developed iSAM algorithms could be an interesting alternative [31]–[33], which will be considered for this problem.

ACKNOWLEDGEMENT

This work was supported by ONR MURI Grant N000141110688.

REFERENCES

[1] J. C. Latombe, *Robot Motion Planning*. Kluwer Academic Publishers, 1991.

[2] S. Ferrari, C. Cai, R. Fierro, and B. Perteet, "A multi-objective optimization approach to detecting and tracking dynamic targets in pursuit-evasion games," in *Proc. of American Control Conference*, July 11-13 2007.

[3] D. Culler, D. Estrin, and M. Srivastava, "Overview of sensor networks," *Computer*, vol. 37, no. 8, pp. 41–49, 2004.

[4] P. Juang, H. Oki, Y. Wang, M. Martonosi, L. Peh, and D. Rubenstein, "Energy efficient computing for wildlife tracking: Design tradeoffs and early experiences with zebranet," in *Proc. of 10th International Conference on Architectural Support for Programming Languages and Operating Systems (ASPLOS-X)*, October 2002.

[5] W. Lu, G. Zhang, S. Ferrari, R. Fierro, and I. Palunko, "An information potential approach for tracking and surveilling multiple moving targets using mobile sensor agents," in *Proc. of SPIE Defense, Security, and Sensing*. Orlando, Florida, United States: International Society for Optics and Photonics, April 2011, pp. 80 450T–80 450T.

[6] W. Lu, G. Zhang, and S. Ferrari, "A comparison of information theoretic functions for tracking maneuvering targets," in *Proc. of Statistical Signal Processing Workshop (SSP), 2012 IEEE*, August 2012, pp. 149–152.

[7] P. Cheng, G. Pappas, and V. Kumar, "Decidability of motion planning with differential contraints," in *Proc. of the 46nd IEEE International Conference on Robotics and Automation*, Roma Italy, March 2007, pp. 1826–1831.

[8] S. Ferrari, R. Fierro, B. Perteet, C. Cai, and K. Baumgartner, "A geometric optimization approach to detecting and intercepting dynamic targets using a mobile sensor network," *SIAM Journal on Control and Optimization*, vol. 48, no. 1, pp. 292–320, 2009.

[9] X. Zhou, K. X. Zhou, and S. Roumeliotis, "Optimized motion strategies for localization in leader-follower formations," in *Proc. of Intelligent Robots and Systems (IROS), 2011 IEEE/RSJ International Conference on*, Sept 2011, pp. 98–105.

[10] F. Morbidi and G. Mariottini, "Active target tracking and cooperative localization for teams of aerial vehicles," *Control Systems Technology, IEEE Transactions on*, vol. 21, no. 5, pp. 1694–1707, Sept 2013.

[11] S. Ferrari and C. Cai, "Information-driven search strategies in the board game of clue," *Systems, Man, and Cybernetics - Part B, IEEE Transactions on*, vol. 39, no. 3, pp. 607–625, 2009.

[12] C. Cai and S. Ferrari, "Information-driven sensor path planning by approximate cell decomposition," *IEEE Transactions on Systems, Man, and Cybernetics - Part B*, vol. 39, no. 3, pp. 607–625, 2009.

[13] G. Zhang, S. Ferrari, and M. Qian, "An information roadmap method for robotic sensor path planning," *Journal of Intelligent and Robotic Systems*, vol. 56, pp. 69–98, 2009.

[14] W. Lu, G. Zhang, and S. Ferrari, "A randomized hybrid system approach to coordinated robotic sensor planning," in *Decision and Control (CDC), IEEE Conference on*, Atlanta, Georgia, USA, Dec 2010, pp. 3857–3864.

[15] Y. K. Hwang and N. Ahuja, "A potential field approach to path planning," *Robotics and Automation, IEEE Transactions on*, vol. 8, no. 1, pp. 23–32, 1992.

[16] H. Wei and S. Ferrari, "A geometric transversals approach to analyzing the probability of track detection for maneuvering targets," *Computers, IEEE Transactions on*, vol. PP, no. 99, pp. 1–1, 2013.

[17] K. Baumgartner and S. Ferrari, "A geometric transversal approach to Analyzing track coverage in sensor networks," *Computers, IEEE Transactions on*, vol. 57, no. 8, pp. 1113 –1128, 2008.

[18] V. Isler, C. Belta, K. Daniilidis, and G. J. Pappas, "Hybrid control for visibility-based pursuit-evasion games," in *Proc. of Intelligent Robots and Systems (IROS), IEEE/RSJ International Conference on*, vol. 2, Sendai, Japan, Sept 2004, pp. 1432–1437.

[19] L. Lulu and A. Elnagar, "A comparative study between visibility-based roadmap path planning algorithms," in *Proc. of the Conference on Intelligent Robots and Systems (IROS), IEEE/RSJ International Conference on*, Aug 2005.

[20] S. Bhattacharya, R. Murrieta-Cid, and S. Hutchinson, "Optimal paths for landmark-based navigation by differential-drive vehicles with field-of-view constraints," *Robotics, IEEE Transactions*, vol. 23, no. 1, pp. 47–59, 2007.

[21] H. Wei, W. Lu, and S. Ferrari, "An information value function for nonparametric gaussian processes," in *Neural Information Processing Systems workshop on Bayesian Nonparametric Models For Reliable Planning And Decision-Making Under Uncertainty*. Lake Tahoe, NV: NIPS, 2012.

[22] M. Baumann, S. Léonard, E. Croft, and J. Little, "Path planning for improved visibility using a proabbilistic road map," *Robotics, IEEE Transactions on*, vol. 26, no. 1, pp. 195–200, 2010.

[23] P. Zhu, B. Chen, and J. C. Príncipe, "Extended Kalman filter using a kernel recursive least squares observer," in *Proc. of Neural Networks (IJCNN), The 2011 International Joint Conference on*, San Jose, California, USA, Aug 2011, pp. 1402–1408.

[24] K. Zhou and S. I. Roumeliotis, "Multirobot active target tracking with combinations of relative observations," *Robotics, IEEE Transactions on*, vol. 27, no. 4, pp. 678–695, 2011.

[25] P. Zhu, B. Chen, and J. C. Príncipe, "A novel extended kernel recursive least squares algorithm," *Neural Networks*, vol. 32, no. 0, pp. 349 – 357, 2012.

[26] E. H. Spanier, *Algebraic topology*. Springer, 1994, vol. 55, no. 1.

[27] H. Wei, W. Ross, S. Varisco, P. Krief, and S. Ferrari, "Modeling of human driver behavior via receding horizon and artificial neural network controllers," in *Decision and Control (CDC), IEEE Annual Conference on*, Florence, Italy, Dec 2013, pp. 6778–6785.

[28] G. P. Huang, K. X. Zhou, N. Trawny, and S. I. Roumeliotis, "Bearing-only target tracking using a bank of MAP estimators," in *Robotics and Automation (ICRA), IEEE International Conference on*, Shanghai, China, May 2011, pp. 4998–5005.

[29] G. Welch and G. Bishop, "An introduction to the kalman filter," 1997.

[30] C. F. Gerald and P. O. Wheatley, *Numerical analysis*. Addison Wesley, 2003.

[31] G. Huang, R. Truax, M. Kaess, and J. J. Leonard, "Unscented iSAM: A consistent incremental solution to cooperative localization and target tracking," in *Mobile Robots (ECMR), European Conference on*. Barcelona, Catalonia, Spain: IEEE, Sept 2013, pp. 248–254.

[32] M. Kaess, A. Ranganathan, and F. Dellaert, "iSAM: Incremental smoothing and mapping," *Robotics, IEEE Transactions on*, vol. 24, no. 6, pp. 1365–1378, 2008.

[33] M. Kaess, H. Johannsson, R. Roberts, V. Ila, J. J. Leonard, and F. Dellaert, "iSAM2: Incremental smoothing and mapping using the bayes tree," *The International Journal of Robotics Research*, vol. 31, no. 2, pp. 216–235, 2012.